3-2019

A Cleft Lip and Palate Gene, Irf6, is Involved in Osteoblast Differentiation of Craniofacial Bone

Jake Thompson
University of Texas Health Science Center at Houston

Fabian Mendoza
University of Texas Health Science Center at Houston

Ethan Tan
University of Texas Health Science Center at Houston

Jessica Wildgrube Bertol
University of Texas Health Science Center at Houston

Arju S. Gaggar
University of Texas Health Science Center at Houston

See next page for additional authors

Recommended Citation

Thompson, J., Mendoza, F., Tan, E., Bertol, J. W., Gaggar, A. S., Jun, G., Biguetti, C., & Fakhouri, W. D. (2019). A cleft lip and palate gene, Irf6, is involved in osteoblast differentiation of craniofacial bone. Developmental dynamics : an official publication of the American Association of Anatomists, 248(3), 221–232. https://doi.org/10.1002/dvdy.13

Authors

Jake Thompson, Fabian Mendoza, Ethan Tan, Jessica Wildgrube Bertol, Arju S. Gaggar, Goo Jun, Cláudia Cristina Biguetti, and Walid Fakhouri

HHS Public Access

Author manuscript

Dev Dyn. Author manuscript; available in PMC 2020 March 01.

Published in final edited form as:

Dev Dyn. 2019 March ; 248(3): 221–232. doi:10.1002/dvdy.13.

A Cleft Lip and Palate Gene, *Irf6*, is Involved in Osteoblast Differentiation of Craniofacial Bone

Jake Thompson[1], **Fabian Mendoza**[1], **Ethan Tan**[1], **Jessica Wildgrube Bertol**[1], **Arju S Gaggar**[2], **Goo Jun**[2], **Claudia Biguetti**[3], and **Walid D. Fakhouri**[1,4,5,*]

[1]Center for Craniofacial Research, Department of Diagnostic and Biomedical Sciences, School of Dentistry, University of Texas Health Science Center at Houston, Houston, TX, USA.

[2]School of Public Health, University of Texas Health Science Center at Houston, Houston, TX, USA.

[3]Department of Basic Sciences, São Paulo State University (Unesp), School of Dentistry, Araçatuba, SP.

[4]Department of Pediatrics, McGovern Medical School, University of Texas Health Science Center, Houston, TX, USA.

[5]Graduate School of Biomedical Sciences, University of Texas Health Science Center and MD Anderson Cancer Center at Houston, TX, USA.

Abstract

Background: Interferon Regulatory Factor 6 (*IRF6*) plays a critical role in embryonic tissue development including differentiation of epithelial cells. Besides orofacial clefting due to haploinsufficiency of IRF6, recent human genetic studies indicated that mutations in *IRF6* are linked to small mandible and digit abnormalities. The function of IRF6 has been well studied in oral epithelium, however its role in craniofacial skeletal formation remains unknown. In this study, we investigated the role of *Irf6* in craniofacial bone development using comparative analyses between wild-type and *Irf6*-null littermate mice

Results: Immunostaining revealed the expression of IRF6 in hypertrophic chondrocytes, osteocytes and bone matrix of craniofacial tissues. Histological analysis of *Irf6*-null mice showed a remarkable reduction in the number of lacunae, embedded osteocytes in matrices and a reduction in mineralization during bone formation. These abnormalities may explain the decreased craniofacial bone density detected by micro-CT, loss of incisors and mandibular bone abnormality of *Irf6*-null mice. To validate the autonomous role of IRF6 in bone, extracted primary osteoblasts from calvarial bone of WT and *Irf6*-null pups showed no effect on osteoblastic viability and proliferation. However, a reduction in mineralization was detected in *Irf6*-null cells.

Conclusions: Altogether, these findings suggest an autonomous role of *Irf6* in regulating bone differentiation and mineralization.

*Correspondence to: Walid D. Fakhouri, PhD, Center for Craniofacial Research, Department of Diagnostic and Biomedical Sciences, School of Dentistry, University of Texas Health Science Center at Houston, Houston, TX 77054, USA, Walid.D.Fakhouri@uth.tmc.edu.

The authors declare that no conflict of interest exists.

Keywords

Craniofacial skeleton; mice; primary osteoblast; chondrocyte; micro-CT

Introduction

Interferon Regulatory Factor 6 encodes for a transcription factor that regulates the expression of interferons and other target genes that are critical for immune function and wound healing (Taniguchi et al., 2001; Tamura et al., 2008; Savitsky et al., 2010). Unlike the rest of the IRF family members, *IRF6* is necessary for craniofacial morphogenesis and ectodermal formation during embryonic development (Ingraham et al., 2006; Richardson et al., 2006). Previous studies had investigated its function in epithelial proliferation and differentiation (Ingraham et al., 2006; Knight et al., 2006; Richardson et al., 2006) and confirmed its dynamic expression in ectoderm, periderm, oral epithelium and tooth germ in embryonic tissues (Blackburn et al., 2012; Fakhouri et al., 2012). Apart from its ectodermal role, IRF6 has been shown to regulate human erythropoiesis and immune cells, namely neutrophils, macrophages and dendritic cells (Joly et al., 2016; Xu et al., 2012). These biological processes occur in the bone marrow and lymphatic system to provide protection against pathogens that activate Toll-like receptors (Kwa et al., 2014; Joly et al., 2016). Expression of IRF6 in epithelial cells is necessary during embryonic development because loss of expression has been implicated in genetic birth defects such as Van der Woude (VWS) and Popliteal Pterygium syndromes (PPS) (Kondo et al., 2002; Gritli-Linde, 2008). These birth defects are characterized by a cleft lip with or without cleft palate, as well as skin and dental abnormalities (Kondo et al., 2002).

Patients with VWS have other clinical features that are frequently associated with orofacial cleft and lip pits including hypodontia in 20–40% of cases, narrow arched palatal bone, clubfoot, and cerebral abnormalities (Kondo et al., 2002; Rizos and Spyropoulos, 2004). Moreover, syngnathia and rib abnormalities have been reported in severe cases of PPS (Escobar and Weaver, 1978; Cardoso et al., 1998; Vandeweyer et al., 2000). Similarly, a complete loss of *Irf6* in mice leads to skeletal abnormalities, including xiphoid and digits malformation (Ingraham et al., 2006; Fakhouri et al., 2017), while exogenous overexpression of IRF6 in basal epithelium partly rescued the craniofacial phenotype in *Irf6* null embryos (Kousa et al., 2017). Despite all these findings, no studies have reported IRF6 expression in osteogenic cells during bone formation (Fakhouri et al., 2017; Manocha et al., 2018). Our recently published study showed that IRF6 is not expressed in migratory cranial neural crest cells, however it regulates the expression of Endothelin 1 ligand (Edn1) in the mandibular epithelium which binds at Edn1-receptors expressed in adjacent mesenchymal cells to stimulate the cell differentiation (Fakhouri et al., 2017). These findings suggest that IRF6 is involved in bone and cartilage formation in a cell non-autonomous fashion and that lack of IRF6 causes aberrant skeletal phenotypes that may contribute to micrognathia and cleft palate. Likewise, small mandible or retrognathia leads to a complete cleft palate in patients affected with Pierre Robin sequence (Johnston and Nash, 1982; Laitinen et al., 1997). However, it is currently not well-understood how IRF6, a transcription factor that is

primarily expressed in epithelial cells, could be involved in the development of bone and cartilage during embryogenesis (Duncan et al., 2017).

Bone formation is a highly regulated process starting when the mesenchymal cells become osteoblasts, the cells that contribute to the formation of bone matrix. Importantly, osteoblasts follow a 3-step pathway of development which includes specification, commitment and differentiation into osteocytes that are embedded in newly formed bone matrix (Horton, 1990; Rutkovskiy et al., 2016). Bone matrix mineralization and differentiation of osteoblasts into osteocytes are not a consequential process and that mineralization can occur independently of osteocyte differentiation. Considering a mineralization process involving tooth enamel and dentin in the craniofacial skeleton affected by lack of *Irf6*, recent studies showed that tooth enamel of *Irf6* conditional knockout by the *Pitx2-Cre* driver line showed delayed maturation and aberrant organization of enamel and dentin forming cells (Chu et al., 2016; Tamasas and Cox, 2016). In alignment with a potential cell-autonomous role in bone formation, a recent report showed that in individuals affected with orofacial clefting, IRF6 was detected in mature chondrocytes and a few osteocytes of nasal bone tissues (Krivicka-Uzkurele and Pilmane, 2016).

Considering the expansive spectrum of action IRF6 has during embryonic and fetal development, this study investigated the function of *Irf6* in intramembranous craniofacial bone development during embryonic development at early and late stages due to the abnormal skeletal phenotype observed in *Irf6*-null mice. We investigated the expression of IRF6 in craniofacial bone and cartilage cells at multiple embryonic stages. Understanding the importance of IRF6 in craniofacial bone and cartilage development will not only help in extending our current knowledge of this gene's function but will also have significant implications for the precise diagnosis and prognosis of skeletal defects and late-onset disorders. This study sought to determine the underlying mechanism of *Irf6* function in craniofacial bone development by comparative analysis using 3D micro-CT, histomorphological and immunostaining analysis, as well as *in vitro* primary cell-based assays.

Results

Expression of IRF6 in Enamel Organ, Bone Matrix and Hypertrophic Chondrocytes

We conducted immunohistochemical staining of mouse head cross sections to determine the expression in embryonic bone and cartilage tissues. In newly formed bone matrices, as observed in mandibular bone, IRF6 was expressed in the osteocytes of developing intramembranous alveolar bone surrounding the mandibular tooth germ and in proximity to dental papilla (Fig. 1A, A'). The expression of IRF6 was also detected in developing mandibular regions containing fully-formed bone matrices and hypertrophic chondrocytes of Meckel's cartilage (Fig. 1B-B'). Further supporting the expression in differentiated chondrocytes, the IHC staining also revealed that IRF6 was markedly expressed in hypertrophic chondrocytes of nasal cartilage (Fig. 1C-C'). Nasal cartilage shows the resting, proliferating, and hypertrophic zone of nasal cartilage and the zone of calcified bone (Fig. 1C-C'). Immunofluoresent staining also confirmed the expression of IRF6 in alveolar bone cells (Fig. 1D, D') and dentary bone (Fig. 1E) of the mandible, and showed that the

expression is mainly localized in the cytosol of bone cells of wild-type embryos. Also, few bone and cartilage cells showed nuclear expression of IRF6 (Fig. 1B', D').

Effect of Early Embryonic Bone Development

Goldner's Trichrome-Alcian Blue staining was used to observe new skeletal structure formation and bone matrix mineralization during embryonic and fetal development. At E13.5, coronal sections of WT (Fig. 2A, A') and *Irf6*-null heads (Fig. 2C, C') were stained and showed no remarkable difference in the tissues that give rise to bone structure. However, the Meckel's cartilage of the mandible was relatively more compact with chondrocytes and had less intercellular space in *Irf6*-null mice (Fig. 2C'). However, quantitative analysis of the number of chondrocytes within the Meckel's cartilage of the wild-type and *Irf6*-null was performed for a total of 6 samples and the average number did not show a significant difference (Fig. 2I). At older stages, the variations in differentiated Meckel's cartilage were more obvious showing larger and more vacuolated hypertrophic chondrocytes in WT (Fig. 2B), while in *Irf6*-null mice the cartilage showed more condensed matrices and has fewer vacuolated hypertrophic chondrocytes (Fig. 2D). In WT mandibular bone, the embryonic tissues at E15.5 showed organized newly formed bone matrices surrounding the Meckel's cartilage (Fig. 2E) where osteocytes were trapped in osteogenic lacunae (Fig. 2E'). In *Irf6*-null, mandibular bone had remarkably fewer osteocytes embedded in the newly formed bone matrices as well as a disruption of the matrix structure at E15.5 (Fig. 2G, G'). Quantitative analysis of the number of osteocytes embedded in mandibular bone matrix showed a significant reduction in the average number of osteocytes in *Irf6*-null mandible compared to wild-type littermates (Fig. 2J).

The same staining procedure was also used to determine the mineralization of bone matrices at later time points. At E17.5, the stain of bone matrices changed from green to red as the matrix became more mineralized in WT (Fig. 2F), while the stain remained green in *Irf6*-null tissues, suggesting a lack or delayed mineralization of mandibular bone matrices (Fig. 2H).

Histomorphological Phenotype in *Irf6*-null Craniofacial Bone Structure

H&E staining was performed to detect histological changes in mandibular components of WT and *Irf6*-null mice at P0 (Fig. 3A, C). The stained sections showed that the periosteum of *Irf6*-null mandible was morphologically irregular with a lobulated outer layer, and the trabecular bone matrix was disorganized with large void areas (Fig. 3C) compared to WT (Fig. 3A). To visualize calcified bone matrices, von Kossa staining was performed in WT, which showed organized and connected matrices of trabecular mandibular bone (Fig. 3B, B'). In *Irf6*-null mandibular tissues, the bone matrices were dispersed and disconnected (Fig. 3D, D'). The osseous tissues of *Irf6*-null mice showed aberrant organization of bone matrix especially at the distal region of the mandible. Furthermore, the incisor roots of lower jaw were missing (Fig. 3D). To investigate whether the disorganized matrices are due to disruption of bone remodeling, immunostaining of TRAP (ACP5) showed enrichment of TRAP+ osteoclasts along the new bone matrix in WT (Fig. 3E), while the number of stained TRAP+ osteoclasts was qualitatively reduced in *Irf6*-null tissues of the mandible (Fig. 3F). The number of TRAP+ osteoclasts detected by the IHC staining was counted and showed a

significant reduction in *Irf6*-null samples in comparison to the wild-type littermates (Fig. 3O). Alkaline phosphatase (ALP) assay was preformed to specify whether the osteogenic phenotype in *Irf6*-null is due to alteration of the enzymatic activity of the osteoblasts. The staining of ALP in mandibular WT and *Irf6*-null tissues did not show a remarkable difference in the intensity level (Fig. 3G, H). Skeletal preparation of WT and *Irf6*-null neonatal pups was also performed to determine the macroscopic aberration in the skeleton due to lack of IRF6 expression. Compare to the WT newborn skeleton of the bone and cartilage (Fig. 3I, L), *Irf6*-null heads had multiple skeletal defects including mandibular abnormalities (Fig. 3L). The incisors of the upper and lower jaws were missing in *Irf6*-null mice compared to wild-type littermates (Fig. 3J, M), and the distal part of mandibular bone was abnormal in *Irf6*-null mice (Fig. 3N, black arrow). In addition, the symphysis and the mandibular processes of *Irf6*-null mice were abnormal compared to wild-type littermates (Fig. 3K, N). In contrast, these structures were properly formed in WT littermates (Fig. 3J, K). To assess the tissue components of WT and *Irf6*-null mandibular tissues, histomorphometric analysis was utilized at E17.5 and P0 (Fig. 4). The results from the analysis showed that the area density occupied by osteoblasts in *Irf6*-null was not different compared to WT at E17.5, but the percentage was significantly reduced at P0 compared to WT (Fig. 4A). However, the area density of osteocytes in *Irf6*-null was significantly reduced at E17.5 but not at P0 compared to WT (Fig. 4B). No statistical differences were detected in the number of osteoclasts due to large variations among the sections in the wild-type tissues (Fig. 4C) although the immunostaining of TRAP+ osteoclasts showed enrichment in the WT compared to *Irf6*-null littermates. For bone matrix, the area density was significantly reduced in *Irf6*-null at E17.5 and P0 compared to WT (Fig. 4D), while the blood vessels showed significant reduction only at P0 in *Irf6*-null compared to WT (Fig. 4E). However, the other tissue components were significantly increased in *Irf6*-null at P0 compared to WT (Fig. 4F).

Lack of IRF6 Leads to Craniofacial Bone Abnormalities

3D rendering images of micro-CT scans revealed dense areas for newborn WT heads compatible with normal bone structure of the skull, nasal bones, and jaws (Fig. 5A – 1st and 2nd rows), while *Irf6*-null heads showed jaw abnormalities and fewer mineralized bone of the skull (Fig. 5A – 3rd and 4th rows). Early fusion between the parietal and frontal skull bones at the coronal junction and between parietal and temporal bones at the squamosal suture were observed in *Irf6*-null mice compared to unfused sutures in WT (Fig. 5A, 4th row, blue arrow). Although, craniosynostosis between the parietal and frontal skull bones was reported in our previous study of *Irf6*-null mice (Fakhouri et al., 2017), no data was provided on the expression or function of IRF6 in bone and cartilage formation. Detached remnants of incisors and abnormal mandibular bone were observed in *Irf6*-null pups (Fig. 5A, blue arrow in last column). Analysis of the 3D rending images showed that the total volumes (mm^3) of frontal (Fig. 5B) and mandibular (Fig. 5C) bone were smaller in *Irf6*-null mice compared to WT littermates. The 3D rendering images are representative of 2 individual pups of WT and *Irf6*-null littermate mice.

Autonomous Effect on Osteoblasts

To further delve into the autonomous function of IRF6 during bone development and mineralization, calvarial primary cells were harvested from frontal bone of fresh newborn WT (Fig. 6A) and *Irf6*-null skulls (Fig. 6B) to evaluate cell proliferation in non-differentiation medium and for the mineralization potency in differentiation medium. Images taken 24h following isolation of calvarial cells showed no visible differences between the WT (Fig. 6C) and *Irf6*-null cell cultures regarding the number of adhered cells (Fig. 6F). In addition, prior to mineralization and after 7 days of cultivation, both WT and *Irf6*-null cell cultures completely proliferated into confluence without any differences in timing (Fig. 6D, G). Once cells reached confluence, the medium was replaced with differentiation medium and the cells were grown for another 2 and 3 weeks. Staining with alizarin red resulted in noticeable dispersed mineralized foci between the WT and *Irf6*-null cultured wells. Following two weeks in differentiation medium, alizarin red staining showed that WT had large mineral deposit foci (Fig. 6E) in comparison to the *Irf6*-null that showed tiny mineral deposit foci (Fig. 6H). The difference in the mineralization was also observed macroscopically with the WT showing denser mineralized structures compared to *Irf6*-null cells. Three weeks after incubation, another batch of cells at 10K per well were stained for mineralization with similar results observed apart from the level of mineralization, suggesting a delay or disruption of the mineralization process due to loss of IRF6 in primary osteogenic cells (Fig. 6I). Although the level of mineralization was notably not different at higher cell concentrations per well at both 15K and 20K, the mineralized foci of *Irf6*-null cells were slightly dispersed in 15K wells (Fig. 6I). However, the *in vitro* pattern of alizarin staining can depend on the seeding procedure of primary cells and is not necessarily due to intrinsic factors. Collectively, this data further suggests an autonomous role of IRF6 in osteogenic primary cell mineralization. To confirm the expression of the *Irf6* gene in extracted bone cells, we conducted western blot analysis in extracted primary cells. The WT bone cells grown in normal (WT) and differentiation media (D-WT) for 3 weeks expressed IRF6 protein, while no protein band specific to IRF6 was detected in *Irf6*-null cells (MT and D-MT), as expected (Fig. 6J). Total protein extracted from murine skin was served as a positive control for IRF6 protein expression.

Differentially Altered Gene Expression

Previous studies showed that IRF6 is involved in the innate immune system, wound healing of ectoderm, and keratinocyte differentiation (Ingraham et al., 2006; Kwa et al., 2014; Joly et al., 2016). Therefore, we hypothesized that loss of *Irf6* in bone cells disrupts the expression of genes involved in osteoclastogenesis and osteoblast differentiation. To test this hypothesis, relative RTqPCR was utilized to investigate 29 candidate genes that were selected based on their involvement in bone formation and immune system. Based on the relative normalized expression of 29 genes in *Irf6*-null and WT mice, the 10 most differentially expressed genes were measured using quantitative standard curve by RTqPCR. The transcriptional levels of these 10 genes were normalized to the house-keeping gene *Gapdh* that was not altered in *Irf6*-null tissues compared to WT (Fig. 7). The normalized gene expression data showed that *Cxcl12*, a chemokine expressed by mesenchymal osteoprogenitor cells and endothelial cells to regulate bone remodeling (Shahnazari et al., 2013), was significantly upregulated in *Irf6*-null compared to WT. Similarly, *IL-10*, a

cytokine involved in the downregulation of the receptor activator of NF-κB ligand (RANKL) expression and osteoclastogenesis (Zhang et al., 2014), and *Irf4,* a transcription factor dimerizes with IRF6 and regulates *Ccl17* expression, were significantly upregulated in *Irf6*-null compared to WT (Fig. 7). In contrary, *Ccl17* and *Rankl* expression were downregulated in *Irf6*-null compared to WT. *Foxn4* and *Helt*, developmental transcription factors involved in the development of the nervous system (Del Barrio et al., 2007; Tassopoulou-Fishell et al., 2012)., were both significantly upregulated in *Irf6*-null mandibular tissues compared to WT (Fig. 7).

Discussion

This study investigated the function of *Irf6* in craniofacial bone development during embryogenesis. The data presented in this study is the first report that suggests a direct role of *Irf6* in intramembranous bone formation and mineralization. Previous studies had focused on the importance of IRF6 in epithelial cells and wound healing due to the obvious pathologies observed in VWS and PPS patients at birth (Ingraham et al., 2006; Vieira, 2008; Letra et al., 2012; Fakhouri et al., 2014; Joly et al., 2016), though this study concentrated on the effect of IRF6 on craniofacial bone formation due to aberrant skeletal phenotype observed in *Irf6*-null mice (Ingraham et al., 2006) and dominant negative Irf6 in zebrafish (Duncan et al., 2017). Although our previous study suggested an intercellular role of IRF6 which is highly expressed in epithelial cells on mandibular bone development (Fakhouri et al., 2017), no studies thus far have investigated whether IRF6 is involved in regulating bone and cartilage development in a cell-autonomous manner. Interestingly, our finding of IHC staining extended the knowledge about the current perception of IRF6's role in intramembranous bone formation by reporting the distinct expression in intramembranous differentiated osteogenic cells, and in hypertrophic chondrocytes of Meckel's and nasal cartilage. The IHC finding further support an autonomous effect on craniofacial bone formation and is consistent with a recently published study reporting that IRF6 expression was detected in the cartilage and bone of secondary palatal tissues obtained from patients affected with the common form of cleft palate (Krivicka-Uzkurele and Pilmane, 2016). IRF6 expression in hypertrophic chondrocytes might suggest a role in the ossification of hypertrophic zone of craniofacial bone development, a process that takes place at the condyle and other mandibular processes (Mackie et al., 2008). Notably, our data of 3D micro-CT images and skeletal staining showed that the mandibular processes (angular and coronoid) of *Irf6*-null mice are moderately aberrant compared to wild-type littermates. Furthermore, IRF6 expression was detected in the regions of developing mineralized structures like tooth enamel although these structures are derived from odontogenic ectomesenchyme. Consistent with the cell-type expression and associated phenotype, the micro-CT and skeletal staining data showed that lack of IRF6 expression leads to deformed or missing incisors, abnormal mandibular shape and structure. Lacking of incisors in *Irf6*-null embryos could have an effect on alveolar bone formation and development. Yet, bone abnormalities were observed not only in alveolar bone but also in dentary bone and skull.

Based on the macroscopic phenotype, we investigated the histological features resulted from IRF6 deficiency in mandibular tissues to determine which cell types and structures are affected in craniofacial tissues. Our data showed that fewer osteocytes were detected in

newly formed bone of *Irf6*-null mandibular tissues at E17.5, as well as delayed or reduced level of mineralized bone matrix in *Irf6*-null at E17.5 and P0 time points. The histological and skeletal staining data are in agreement with the 3D micro-CT of *Irf6*-null pups which showed a reduced bone volume and abnormal mandibular structure. Collectively, the expression in bone cells and the bone pathology further suggest an autonomous role of IRF6 in regulating the formation of intramembranous craniofacial bone.

Importantly, the *in vitro* primary osteogenic cell assay is consistent with the *in vivo* observations for an intrinsic role of IRF6 in osteogenic cell differentiation and mineralization by which loss of IRF6 leads to less bone volume and mineralization. The *in vitro* osteogenic assay showed that IRF6 is not critical for primary bone cell proliferation, but it is important for the mineralization process. The 3D micro-CT and *in vitro* data indicated that *Irf6*-null mice were delayed in bone maturation, and hence the calvarial primary cells that were extracted from frontal skull bone were less mature to start with or the mineralization process was altered. This is consistent with the IHC data that showed a reduced average number of embedded osteoclasts in *Irf6*-null tissues compared to WT mandibular tissues. The late endogenous IRF6 expression until bone cells are deposited into the matrix may explain how its role, though direct, may only be involved in the terminal steps of the bone maturation. The IRF6 protein expression in cultured primary osteogenic cells was also detected 3 weeks post-incubation in both the normal and differentiation media.

Recent human genetic studies have indicated that mutations in *IRF6* gene are associated with craniofacial bone pathology. Notably, a novel missense mutation in IRF6 coding region was identified in a multigenerational familial cohort diagnosed with cleft lip and palate and Pierre Robin sequence (PRS) in which the affected individual has very short mandible and complete cleft of secondary palate (Pengelly et al., 2015). Similarly, other human genetic studies reported that patients with Popliteal Pterygium syndrome caused by IRF6 dominant negative mutations also suffer from small mandible (Escobar and Weaver, 1978; Mahalik and Menon, 2010). Furthermore, mutations in *IRF6* had been linked to craniofacial and brain abnormalities in patients affected with van der Woude syndrome and idiopathic growth hormone deficiency (Oberoi and Vargervik, 2005; Nopoulos et al., 2007; Starink et al., 2017). Consistent with these findings, our previous study showed that *Irf6* genetically interacts with *Twist1* during craniofacial bone development and that the compound heterozygous mice for *Irf6* and *Twist1* have severe micrognathia (Vieira et al., 2007; Song et al., 2013; Fakhouri et al., 2017).

The observations of decreased mineralization in *Irf6*-null mice carry significant implications in the pathology of various skeletal and dental diseases. Recent studies presented a correlation between DNA mutations in *IRF6* and an increased susceptibility to severe dental caries or tooth agenesis, especially patients with the syndromic cleft lip and palate (Song et al., 2013; Chu et al., 2016; Tamasas and Cox, 2016). Considering mineralized structures of craniofacial tissues like the tooth enamel, a conditional knockout of *Irf6* in the oral epithelium showed delayed maturation and aberrant organization of enamel forming cells, known as ameloblasts (Tamasas and Cox, 2016). The findings of our study could translate into the ameloblasts and odontoblasts differentiation in future studies.

Finally, we investigated the differential expression of genes important for craniofacial bone development in *Irf6*-null mandibular tissues to identify potential disrupted gene network. According to previous studies, IRF6 regulates genes that are involved in wound healing and immune system. The differential gene expression data showed that *Helt* and *Foxn4* were significantly upregulated in *Irf6*-null compared to WT mice, as well as *Cxcl12* which might explain the reduction or delayed process of bone cell differentiation. *Cxcl12* is a chemokine expressed by mesenchymal osteoprogenitor cells which is involved in regulating bone remodeling (Shahnazari et al., 2013), while *FoxN4* is a developmental transcription factor located in a susceptible risk locus associated with mandibular prognathism and has an important role in the development of the nervous system (Del Barrio et al., 2007; Tassopoulou-Fishell et al., 2012). Interestingly, the cytokine IL-10, an important molecule involved in the downregulation of the receptor activator of NF-κB ligand (RANKL) and a potent inhibitor of osteoclastogenesis (Zhang et al., 2014), was significantly upregulated in *Irf6*-null embryos, while the resorption markers *Rankl* and *Ccl17* expression were downregulated compared to WT. In agreement with the molecular results for IL10, CCL17 and RANKL, the average number of TRAP+ osteoclasts was significantly reduced in *Irf6*-null samples compared to WT. It has been known that the immune system related molecules play a role in osteoblasts and osteoclasts differentiation along inflammatory response to healing conditions (Vieira et al., 2015). Our results point toward a potential regulatory role of IRF6 and other immune-related molecules along bone formation and modeling during skeleton development, without stimuli from inflammatory response (Miclau et al., 2005).

In conclusion, our data showed that IRF6 is expressed in bone cells and is involved in osteogenic cell differentiation and mineralization in a cell-autonomous mechanism. Additional studies are required to understand the molecular involvement of IRF6 in dental and skeletal defects in order to identify affected regulatory pathway(s) and target genes.

Experimental Procedure

Mice Handling and Generation of *Irf6*-null Embryos

Mice generation on C57BL/6J genetic background and genotyping of *Irf6*-null alleles were performed as previously described (Fakhouri et al., 2017). Craniofacial embryonic development was analyzed at embryonic day (E) 13.5 until P0 comparing wild-type (WT) with *Irf6*-null murine samples. Procedures involving the use of animals were approved by the Animal Welfare Committee (AWC-16–0068) at the University of Texas Health Science Center at Houston and followed the National Institute of Health guidelines.

Micro-CT

The Optical Imaging and Vital Microscopy core at Baylor College of Medicine was used for the 3D rendering of micro-CT scans. A Bruker 1272 micro-CT (SkyScan, Kontich, Belgium) was used to image WT and *Irf6*-null murine embryos at perinatal P0 as previously described (Vieira et al., 2015). Specimens were scanned at a resolution of 12 μm pixel size and intensity of 145μA. Briefly, projected images were reconstructed with NRecon software and subsequently three-dimensional images were obtained by CT-Vox software. This system allowed for non-destructive visualization and imaging capabilities of objects as small as 0.35

μm by means of 3D rendering images adjusted for optimum visualization of hyper-dense areas of craniofacial bones with minimal interference. Two biological replicates of WT and *Irf6*-null littermate pups were scanned for micro-CT (μCT) image analysis and quantification on bone volume. For quantitative analyses, were used guidelines as previously described for μCT characterization (Bouxsein et al., 2010). Bilateral mandibular and frontal bones were segmented in a region of interest (ROI) using CTAn software (Skyscan, Kontich, Belgium) and specimens were evaluated considering the volume [mm3]. Additional μCT scanning was performed for the two pups used in the *in vitro* primary osteoblast extraction. The two pups were incubated in 50% silver nitrate solution and scanned at a resolution of 10 μm pixel size.

Histological Assays

We performed a modified Goldner's Trichrome-Alcian Blue and von Kossa staining to identify newly formed bone matrix and cartilage and mineralized bone according to previous publications (Bialek et al., 2004; Egerbacher et al., 2006; Matsumoto et al., 2012). Hematoxylin was also used as a counter stain for nuclei. We favored the Goldner's Trichrome-Alcian Blue staining because of its wider array of colors and contrast, making it easy to clearly distinguish between the different bone tissue components as previously described (Matsumoto et al, 2012). For this staining, the slides of histological sections were incubated for 30 min at 56 ^{0}C in oven to improve staining quality followed by washing in distilled water for 5 min. The sections were first stained with Alcian Blue for 15 min, then washed 3 times with distilled H_2O for 3 min each time. The histological sections then stained with Hematoxylin Harris for 45 s, rinsed in tap water for 6 min, and followed with one time washing in distilled water for 5 min. Following that, the sections were stained in Fuchsin-Ponceau solution for 30 min, rinsed in 1.0% acetic acid solution for 1 min, stained in Orange G dye for 8 min, rinsed again in 1.0% acetic acid solution for 1 min, and finally stained in Light Green solution for 20 min followed with rinsing in 1.0% acetic acid solution for 1 min. The slides were dehydrated in ascending ethanol solution followed with two washes in xylene for 3 min each time. The slides were mounted with cytoseal solution and imaged using an Olympus light microscope. Quantitative analysis of the number of chondrocytes in Meckel's cartilage was performed on 5 biological replicates of wild-type and *Irf6*-null sections that have similar anatomical landmarks. Similarly, quantitative analysis of number of embedded osteocytes was performed using Goldner's Trichrome-Alcian Blue staining images. Three biological replicates and two technical replicates were used for the wild-type and *Irf6*-null mice.

Immunohistochemical (IHC) and Immunofluorescent (IF) Staining

Tissue samples of embryonic and perinatal mandible were deparaffinized and rehydrated for IHC and IF as previously described (Metwalli et al., 2018). Primary antibodies for IRF6 (Fakhouri et al., 2012) and TRAP (ACP5, sc-376875) were used at a dilution of 1:400 and 1:200, respectively, and then incubated overnight as previously described (Filgueira, 2004). The RTU Streptavidin/Peroxidase complex (PK-7800, Vector Laboratories, Burlingame, CA, USA) and Impact DAB Chromagen (SK4105, Vector PK-7800, Vector Laboratories, Burlingame, CA, USA) were applied for visualizing antigen immunoreactivity. Histological slices were counterstained with Mayer's hematoxylin and cover-slipped with permanent

mounting medium. Quantitative analysis was performed to count the number of TRAP+ osteoclasts in the IHC images. The total number of samples used for this analysis was 4 technical replicates for each genotype.

Alkaline Phosphatase Assay and Skeletal Staining

Mandibular tissue samples were deparaffinized, rehydrated, and processed using the Boehringer Mannheim (BM) purple AP substrate as previously described (Wu et al., 2012). Three biological replicates were used for this assay. To determine the effect IRF6 loss on bone and cartilage, alcian blue and alizarin red skeletal staining was performed on wild-type and *Irf6*-null pups at P0 as described previously (Fakhouri et al., 2017).

Histomorphometric Measurements

For histomorphometric measurements, transverse serial sections of WT and *Irf6*-null mouse heads at E17.5 and P0 development stages were cut at 6 μm thickness and stained with hematoxylin and eosin (H&E) as previously described (Metwalli et al., 2018). Microscopic images were captured at 40X magnification and evaluated by a single calibrated investigator by using a grid of points (with 10 parallel lines and 100 points in a quadrangular area) set in the ImageJ software (Version 1.51, National Institutes of Health, Bethesda, Maryland, USA) as previously described (Bouxsein et al., 2010; Vieira et al., 2015). Briefly, 3 fields of each mandibular region were evaluated and points were counted coinciding with the following components: blood vessels, bone matrix, osteoblasts, osteoclasts (multinucleated cells attached to the bone matrix), osteocytes (incorporated at the lacuna), and other components including empty space, other cells, and cartilage as well as muscle. The results are represented as the mean area density for each evaluated structure. For each time point, six biological replicates were used for the quantitative analysis.

Isolation of Osteoblasts and in Vitro Differentiation

Primary mouse calvarial cells were isolated immediately following birth from five biological replicates of WT and *Irf6*-null pups per published techniques (Nohutcu et al., 1997). Skin was carefully peeled away from skull to cut out calvaria underneath and brain tissue was removed. Calvariae were washed four times in plain α-MEM and digested in α-MEM containing 2 mg/mL collagenase A and 2X trypsin. Three digestions were performed at 37°C for 10 min at 200 rpm, 20 min at 200 rpm, and 60 min at 320 rpm. Digested pieces were filtered through a 70 μm sieve and washed in complete α-MEM containing 10% FBS and 1% PSG. Cells were plated in 12-well plates at 100,000 and 200,000 cells/well. For *in vitro* mineralization, osteoblastic cells were grown to complete confluence for 7 days and incubated in mineralization media composed of complete α-MEM (10% FBS, 1% PSG), 50 μg/ml ascorbic acid, and 10 mM β-glycerophosphate as previously described (Nohutcu et al., 1997). The osteoblastic differentiation took up to 3 weeks until mineralization was clearly visible.

RTqPCR

Quantitative gene expression in mandibular tissues was conducted using a Bio-Rad C1000 Touch Thermal Cycler. Primers for differentially expressed genes were ordered from

Integrated DNA technologies. Two biological and 4 technical replicates were used for measuring gene expression.

Statistical Analysis

We performed a multi-variants ANOVA test for the normalized expression data and for the mandibular histomorphometric measurements in WT compared to *Irf6*-null mouse tissues at E17.5 and P0 to determine the significance of any difference among the mean values of different genes. In our experiments, biological replicates from different animals, regardless of whether it is a wild-type or *Irf6*-null, and technical replicates from the same animal were used for the quantitative analysis. For the histomorphometric analysis, we used different number of biological and technical replicates as described before. A p-value less than >0.05 was considered statistically significant.

Acknowledgements

We would like to thank Dr. Franco Cavalla for providing helpful comments and suggestions on the content of this study. We are also grateful to Ishita Akhter for her excellent help with the immunofluorescent staining. The authors specially thank Dr. Laurie McCauley from the University of Michigan School of Dentistry for providing us with the protocol for the cell-autonomous assay in calvarial bone and for reviewing this manuscript. We specially thank Dr. Brian Schutte at Michigan State University for the *Irf6* heterozygous mice used in this study. This study was supported by the Rolanette and Brandon Lawrence Bone Disease Program in Texas. We also thank the support from NIH grant R15GM122030-01 to WDF.

Grant sponsor and number: Rolanette and Brandon Lawrence Bone Disease Program in Texas and NIH grant number: R15GM122030-01.

References

Blackburn J, Ohazama A, Kawasaki K, Otsuka-Tanaka Y, Liu B, Honda K, Rountree RB, Hu Y, Kawasaki M, Birchmeier W, Schmidt-Ullrich R, Kinoshita A, Schutte BC, Hammond NL, Dixon MJ, Sharpe PT. 2012 The role of Irf6 in tooth epithelial invagination. Dev Biol 365:61–70. [PubMed: 22366192]

Bouxsein ML, Boyd SK, Christiansen BA, Guldberg RE, Jepsen KJ, Muller R. 2010 Guidelines for assessment of bone microstructure in rodents using micro-computed tomography. J Bone Miner Res 25:1468–1486. [PubMed: 20533309]

Cardoso ER, Hawary MB, Mahmud S. 1998 A recessively inherited non-lethal form of popliteal pterygium syndrome. Br J Oral Maxillofac Surg 36:138–140. [PubMed: 9643601]

Chu EY, Tamasas B, Fong H, Foster BL, LaCourse MR, Tran AB, Martin JF, Schutte BC, Somerman MJ, Cox TC. 2016 Full spectrum of postnatal tooth phenotypes in a novel Irf6 cleft lip model. J Dent Res 95:1265–1273. [PubMed: 27369589]

Del Barrio MG, Taveira-Marques R, Muroyama Y, Yuk DI, Li S, Wines-Samuelson M, Shen J, Smith HK, Xiang M, Rowitch D, Richardson WD. 2007 A regulatory network involving Foxn4, Mash1 and delta-like 4/Notch1 generates V2a and V2b spinal interneurons from a common progenitor pool. Development 134:3427–3436. [PubMed: 17728344]

Duncan KM, Mukherjee K, Cornell RA. Liao EC. 2017 Zebrafish models of orofacial clefts. Dev Dyn 246:897–914. [PubMed: 28795449]

Egerbacher M, Helmreich M, Mayrhofer E, Bock P. 2006 Mineralisation of hyaline cartilage in the small-spotted dogfish *Scyliorhinus canicula* L. Scri Med (Brno) 79:199–212.

Escobar V, Weaver D. 1978 Popliteal pterygium syndrome: a phenotypic and genetic analysis. J Med Genet 15:35–42. [PubMed: 633318]

Fakhouri WD, Metwalli K, Naji A, Bakhiet S, Quispe-Salcedo A, Nitschke L, Kousa YA, Schutte BC. 2017 Intercellular genetic interaction between Irf6 and Twist1 during craniofacial development. Sci Rep 7:7129. [PubMed: 28769044]

Fakhouri WD, Rahimov F, Attanasio C, Kouwenhoven EN, Ferreira De Lima RL, Felix TM, Nitschke L, Huver D, Barrons J, Kousa YA, Leslie E, Pennacchio LA, Van Bokhoven H, Visel A, Zhou H, Murray JC, Schutte BC. 2014 An etiologic regulatory mutation in IRF6 with loss- and gain-of-function effects. Hum Mol Genet 23:2711–2720. [PubMed: 24442519]

Fakhouri WD, Rhea L, Du T, Sweezer E, Morrison H, Fitzpatrick D, Yang B, Dunnwald M, Schutte BC. 2012 MCS9.7 enhancer activity is highly, but not completely, associated with expression of Irf6 and p63. Dev Dyn 241:340–349. [PubMed: 22113860]

Filgueira L 2004 Fluorescence-based staining for Tartrate-resistant Acidic Phosphatase (TRAP) in osteoclasts combined with other fluorescent dyes and protocols. J Histochem Cytochem 52:411–414. [PubMed: 14966208]

Gritli-Linde A 2008 Chapter 2, The etiopathogenesis of cleft lip and cleft palate: Usefulness and caveats of mouse models. In: Current Topics in Developmental Biology Academic Press pp 37–138.

Horton WA. 1990 The biology of bone growth. Growth Genet Horm 6:1–3.

Ingraham CR, Kinoshita A, Kondo S, Yang B, Sajan S, Trout KJ, Malik MI, Dunnwald M, Goudy SL, Lovett M, Murray JC, Schutte BC. 2006 Abnormal skin, limb and craniofacial morphogenesis in mice deficient for interferon regulatory factor 6 (Irf6). Nat Genet 38:1335–1340. [PubMed: 17041601]

Johnston L, Nash DJ. 1982 Sagittal growth trends of the development of cleft palate in mice homozygous for the “paddle” gene. J Craniofac Genet Dev Biol 2:265–276. [PubMed: 7183705]

Joly S, Rhea L, Volk P, Moreland JG, Dunnwald M. 2016 Interferon regulatory factor 6 has a protective role in the host response to endotoxic shock. PLoS One 11:e0152385. [PubMed: 27035130]

Knight AS, Schutte BC, Jiang R, Dixon MJ. 2006 Developmental expression analysis of the mouse and chick orthologues of IRF6: The gene mutated in Van der Woude syndrome. Dev Dyn 235:1441–1447. [PubMed: 16245336]

Kondo S, Schutte BC, Richardson RJ, Bjork BC, Knight AS, Watanabe Y, Howard E, Ferreira de Lima RLL, Daack-Hirsch S, Sander A, McDonald-McGinn DM, Zackai EH, Lammer EJ, Aylsworth AS, Ardinger HH, Lidral AC, Pober BR, Moreno L, Arcos-Burgos M, Valencia C, Houdayer C, Bahuau M, Moretti-Ferreira D, Richieri-Costa A, Dixon MJ, Murray JC. 2002 Mutations in IRF6 cause Van der Woude and popliteal pterygium syndromes. Nat Gen 32:285–289.

Kousa YA, Moussa D, Schutte BC. 2017 IRF6 expression in basal epithelium partially rescues Irf6 knockout mice. Dev Dyn 246:670–681. [PubMed: 28643456]

Krivicka-Uzkurele B, Pilmane M. 2016 Expression of interferon regulatory factor 6, muscle segment homeobox 1, paired box gene 9, homeo box B3, and related to tyrosine kinases in human cleft-affected tissue. J Orofac Sci 8:59–65.

Kwa MQ, Nguyen T, Huynh J, Ramnath D, De Nardo D, Lam PY, Reynolds EC, Hamilton JA, Sweet MJ, Scholz GM. 2014 Interferon regulatory factor 6 differentially regulates toll-like receptor 2-dependent chemokine gene expression in epithelial cells. J Biol Chem 289:19758–19768. [PubMed: 24872416]

Laitinen SH, Heliovaara A, Ranta RE. 1997 Craniofacial morphology in young adults with the Pierre Robin sequence and isolated cleft palate. Acta Odontol Scand 55:223–228. [PubMed: 9298165]

Letra A, Fakhouri W, Fonseca RF, Menezes R, Kempa I, Prasad JL, McHenry TG, Lidral AC, Moreno L, Murray JC, Daack-Hirsch S, Marazita ML, Castilla EE, Lace B, Orioli IM, Granjeiro JM, Schutte BC, Vieira AR. 2012 Interaction between IRF6 and TGFA genes contribute to the risk of nonsyndromic cleft lip/palate. PLoS One 7:e45441. [PubMed: 23029012]

Mackie EJ, Ahmed YA, Tatarczuch L, Chen KS, Mirams M. 2008 Endochondral ossification: how cartilage is converted into bone in the developing skeleton. Int J Biochem Cell Biol 40:46–62. [PubMed: 17659995]

Mahalik SK, Menon P. 2010 Popliteal pterygium syndrome. Journal of Indian Association of Pediatric Surgeons 15:110–111. [PubMed: 21124670]

Manocha S, Farokhnia N, Khosropanah S, Bertol JW, Santiago JJ, Fakhouri WD. 2018 Systematic review of hormonal and genetic factors involved in the nonsyndromic disorders of the lower jaw. Dev Dyn 12 21. doi: 10.1002/dvdy.8.

Matsumoto MK, Caviquioli G, Biguetti CC, Holgado LDA, Saraiva PP, Renno´ ACM, Kawakami RY. 2012 A novel bioactive vitroceramic presents similar biological responses as autogenous bone grafts. J Mater Sci Mater Med 23(6):1447–56. [PubMed: 22426745]

Metwalli KA, Do MA, Nguyen K, Mallick S, Kin K, Farokhnia N, Jun G, Fakhouri WD. 2018 Interferon regulatory factor 6 is necessary for salivary glands and pancreas development. J Dent Res 97:226–236. [PubMed: 28898113]

Miclau T, Schneider RA, Frank Eames B, Helms JA. 2005 Common molecular mechanisms regulating fetal bone formation and adult fracture repair Totowa (NJ): Humana Press 45–55 pp.

Nohutcu RM, McCauley LK, Koh AJ, Somerman MJ. 1997 Expression of extracellular matrix proteins in human periodontal ligament cells during mineralization in vitro. J Periodontol 68:320–327. [PubMed: 9150036]

Nopoulos P, Richman L, Andreasen NC, Murray JC, Schutte B. 2007 Abnormal brain structure in adults with Van der Woude syndrome. Clin Genet 71:511–517. [PubMed: 17539900]

Oberoi S, Vargervik K. 2005 Hypoplasia and hypodontia in Van der Woude syndrome. Cleft Palate Craniofac J 42:459–466. [PubMed: 16149825]

Pengelly RJ, Upstill-Goddard R, Arias L, Martinez J, Gibson J, Knut M, Collins AL, Ennis S, Collins A, Briceno I. 2015 Resolving clinical diagnoses for syndromic cleft lip and/or palate phenotypes using whole-exome sequencing. Clin Genet 88:441–449. [PubMed: 25441681]

Richardson RJ, Dixon J, Malhotra S, Hardman MJ, Knowles L, Boot-Handford RP, Shore P, Whitmarsh A, Dixon MJ. 2006 Irf6 is a key determinant of the keratinocyte proliferation-differentiation switch. Nat Gen 38:1329–1334.

Rizos M, Spyropoulos MN. 2004 Van der Woude syndrome: A review. Cardinal signs, epidemiology, associated features, differential diagnosis, expressivity, genetic counselling and treatment. Eur J Orthod 26:17–24. [PubMed: 14994878]

Rutkovskiy A, Stensløkken K-O, Vaage IJ. 2016 Osteoblast differentiation at a glance. Med Sci Monit Basic Res 22:95–106. [PubMed: 27667570]

Savitsky D, Tamura T, Yanai H, Taniguchi T. 2010 Regulation of immunity and oncogenesis by the IRF transcription factor family. Cancer Immunol Immunother 59:489–510. [PubMed: 20049431]

Shahnazari M, Chu V, Wronski TJ, Nissenson RA, Halloran BP. 2013 CXCL12/CXCR4 signaling in the osteoblast regulates the mesenchymal stem cell and osteoclast lineage populations. Faseb J 27:3505–3513. [PubMed: 23704087]

Song T, Wu D, Wang Y, Li H, Yin N, Zhao Z. 2013 SNPs and interaction analyses of IRF6, MSX1 and PAX9 genes in patients with nonsyndromic cleft lip with or without palate. Mol Med Rep 8:1228–1234. [PubMed: 23921572]

Starink E, Hokken-Koelega ACS, Visser TJ, Baan J, Peeters RP, de Graaff LCG. 2017 Genetic analysis of IRF6, a gene involved in craniofacial midline formation, in relation to pituitary and facial morphology of patients with idiopathic growth hormone deficiency. Pituitary 20:499–508. [PubMed: 28593555]

Tamasas B, Cox TC. 2016 Massively increased caries susceptibility in an Irf6 cleft lip/palate model. J Dent Res 96:315–322. [PubMed: 27927890]

Tamura T, Yanai H, Savitsky D, Taniguchi T. 2008 The IRF family transcription factors in immunity and oncogenesis. Annu Rev Immunol 26:535–584. [PubMed: 18303999]

Taniguchi T, Ogasawara K, Takaoka A, Tanaka N. 2001 IRF family of transcription factors as regulators of host defense. Annu Rev Immunol 19:623–655. [PubMed: 11244049]

Tassopoulou-Fishell M, Deeley K, Harvey EM, Sciote J, Vieira AR. 2012 Genetic variation in myosin 1H contributes to mandibular prognathism. Am J Orthod Dentofacial Orthop 141:51–59. [PubMed: 22196185]

Vandeweyer E, Urbain FC, DeMey A. 2000 Facio-genito-popliteal syndrome presenting with bilateral choanal atresia and maxillary hypoplasia. Br J Plast Surg 53:65–67. [PubMed: 10657453]

Vieira AE, Repeke CE, Ferreira Junior Sde B, Colavite PM, Biguetti CC, Oliveira RC, Assis GF, Taga R, Trombone AP, Garlet GP. 2015 Intramembranous bone healing process subsequent to tooth extraction in mice: micro-computed tomography, histomorphometric and molecular characterization. PLoS One 10:e0128021. [PubMed: 26023920]

Vieira AR. 2008 Unraveling human cleft lip and palate research. J Dent Res 87:119–125. [PubMed: 18218836]

Vieira AR, Modesto A, Meira R, Barbosa AR, Lidral AC, Murray JC. 2007 Interferon regulatory factor 6 (IRF6) and fibroblast growth factor receptor 1 (FGFR1) contribute to human tooth agenesis. Am J Med Genet 143a:538–545. [PubMed: 17318851]

Wu T, Zhou H, Hong Y, Li J, Jiang X, Huang H. 2012 miR-30 family members negatively regulate osteoblast differentiation. J Biol Chem 287:7503–7511. [PubMed: 22253433]

Xu J, Shao Z, Glass K, Bauer Daniel E, Pinello L, Van Handel B, Hou S, Stamatoyannopoulos John A, Mikkola Hanna KA, Yuan G-C, Orkin Stuart H. 2012 Combinatorial assembly of developmental stage-specific enhancers controls gene expression programs during human erythropoiesis. Dev Cell 23:796–811. [PubMed: 23041383]

Zhang Q, Chen B, Yan F, Guo J, Zhu X, Ma S, Yang W. 2014 Interleukin-10 inhibits bone resorption: A potential therapeutic strategy in periodontitis and other bone loss diseases. BioMed Res Int 2014:1–5.

Bullet points

- IRF6 is expressed in osteocytes and hypertrophic chondrocytes of craniofacial tissues
- Loss of *Irf6* leads to reduction in the number embedded osteocytes and TRAP + osteoclasts in bone matrices
- *Irf6*-null mice exhibit delay and reduction in bone mineralization, loss of incisors and mandibular hypoplasia

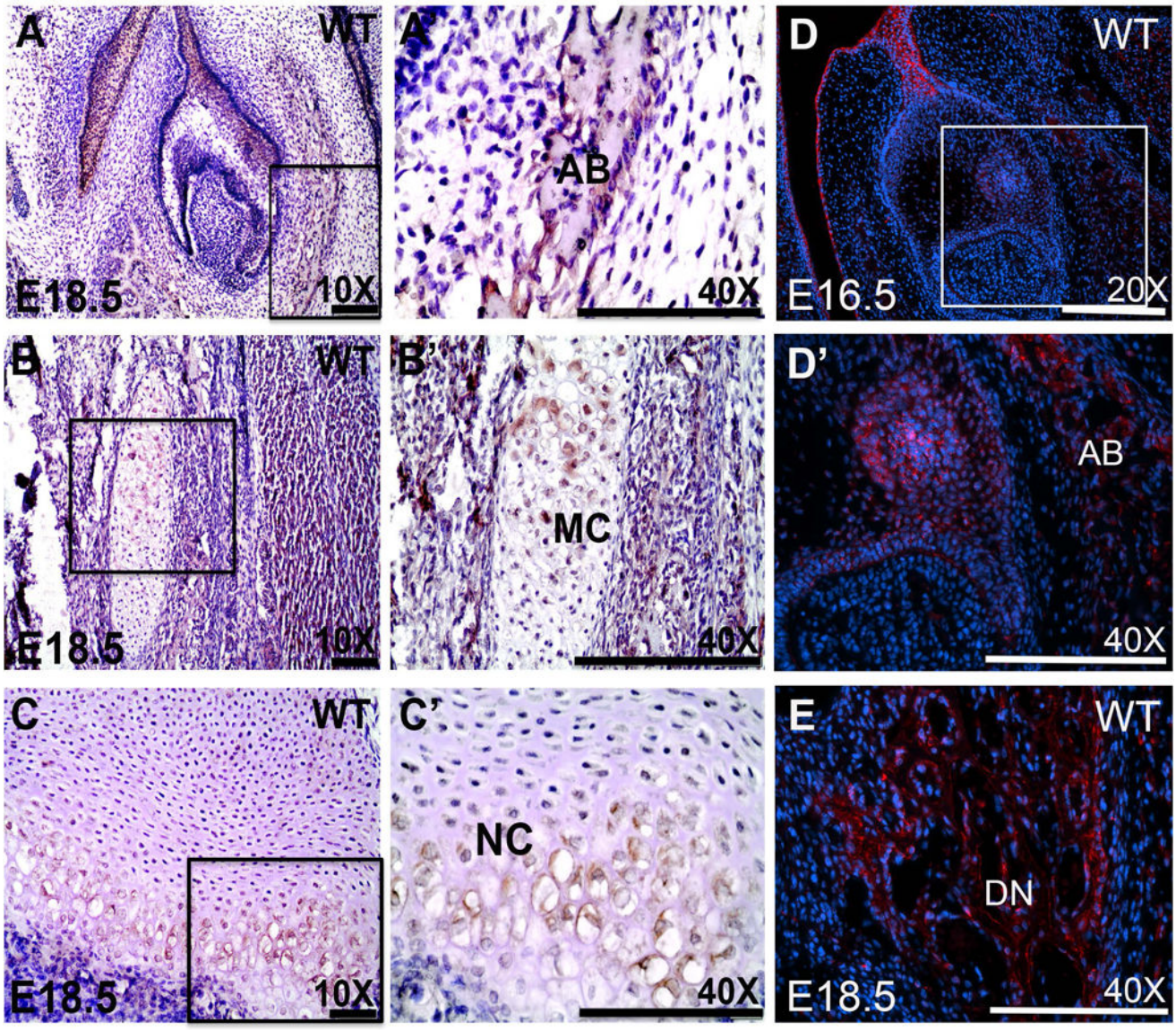

Fig. 1.

Immunohistochemical and immunofluorescent staining of IRF6 in embryonic murine tissues. Expression of IRF6, shown in brown, can be seen in the regions containing mature bone matrices (A, A') and hypertrophic chondrocytes of Meckel's (B, B') and nasal cartilage (C, C') at E18.5. Immunofluorescent staining also shows the expression of IRF6 in alveolar bone cells (D, D') at E16.5 and in dentary bone (E) at E18.5. IRF6 is mainly expressed in the cytosol of bone and cartilage cells as shown by IHC and IF staining. Boxes outline the higher-magnification regions in panels A', B', C' and D'. Wild-type: WT, AB: alveolar bone, DN: dentary, MC: Meckel's Cartilage, NC: nasal cartilage. Scale bars = 100 μm.

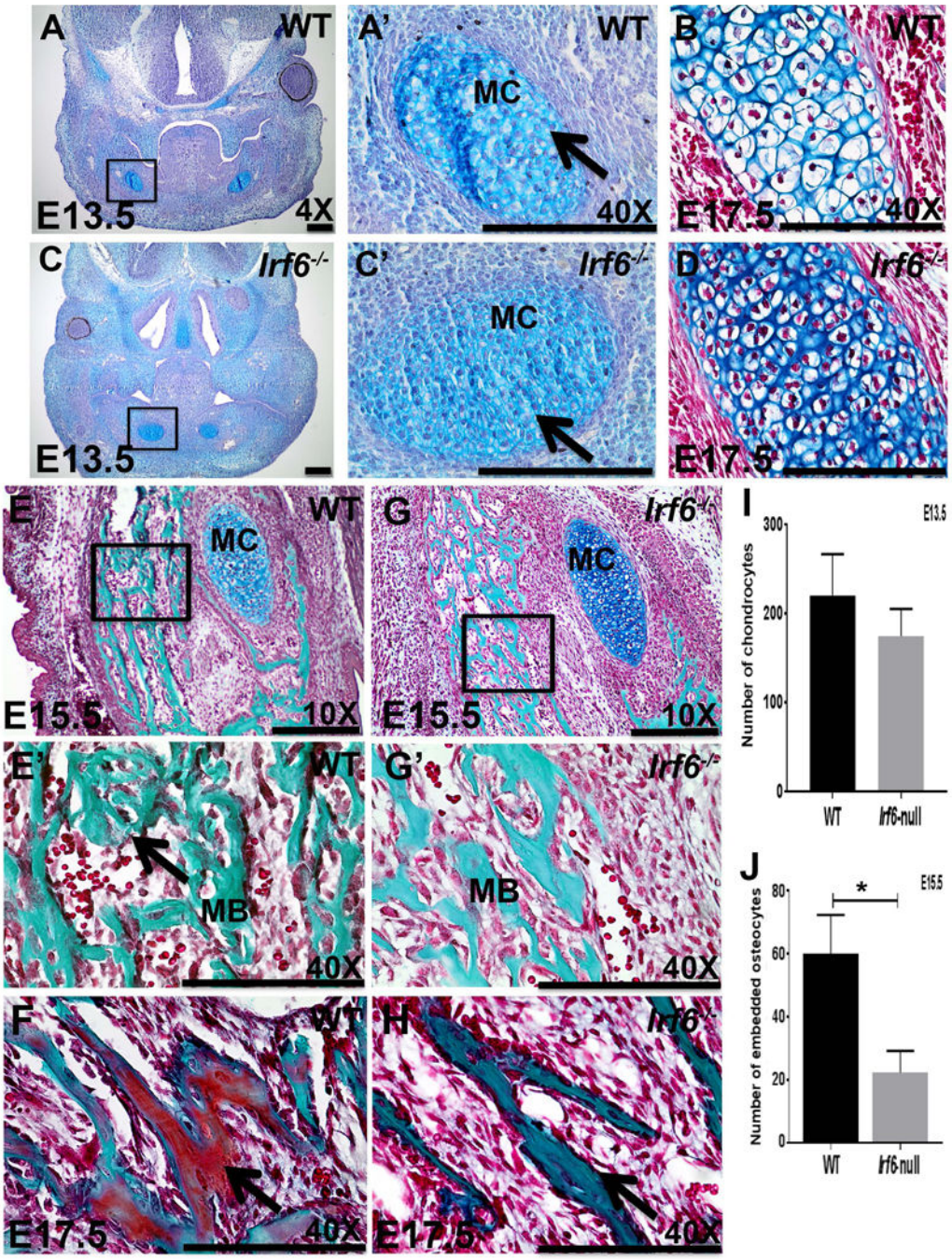

Fig. 2.

Goldner's trichrome-alcian blue staining of WT and *Irf6*-null murine embryonic tissues. At E13.5, coronal sections of wild-type (A, A') and *Irf6*-null (C, C') heads show no remarkable differences except that the cartilage is relatively more condensed with chondrocytes in *Irf6*-null section (C', black arrows). Meckel's cartilage is stained blue, while the surrounding tissues are magenta. At E17.5, the Meckel's cartilage of WT is differentiated into vacuolated hypertrophic chondrocytes (B), while the *Irf6*-null shows fewer vacuolated chondrocytes with blue stained cellular matrices (D). At E15.5, newly formed bone is stained green, while

cartilage is in blue and all other tissue types are stained red in WT (E) and *Irf6*-null (G). In *Irf6*-null sections, fewer osteocytes embedded in the lacunae are observed in the newly formed bone (G') compared to the WT (E'). Mineralization of newly formed bone in green is detected at E17.5 as shown in red color in WT (F, black arrow). No red staining of newly formed bone in *Irf6*-null mandibular tissue is observed suggesting a reduced or delayed mineralization (H, black arrow). Boxes outline the higher-magnification regions in panels A', and C', E' and G'. Number of chondrocytes was counted for 5 biological replicates of wild-type and *Irf6*-null head sections of Meckel's cartilage at E13.5. The average number of chondrocytes is not statistically different between WT and *Irf6*-null (I). Similarly, the number of osteocytes embedded in bone matrix was counted for Goldner's Trichrome-Alcian Blue stained images at E15.5. The average number of osteocytes is significantly reduced in *Irf6*-null compared to WT littermates (J). Wild-type: WT, *Irf6*-null: *Irf6*$^{-/-}$, MC: Meckel's Cartilage, MB: mandibular bone. Scale bars = 100 μm.

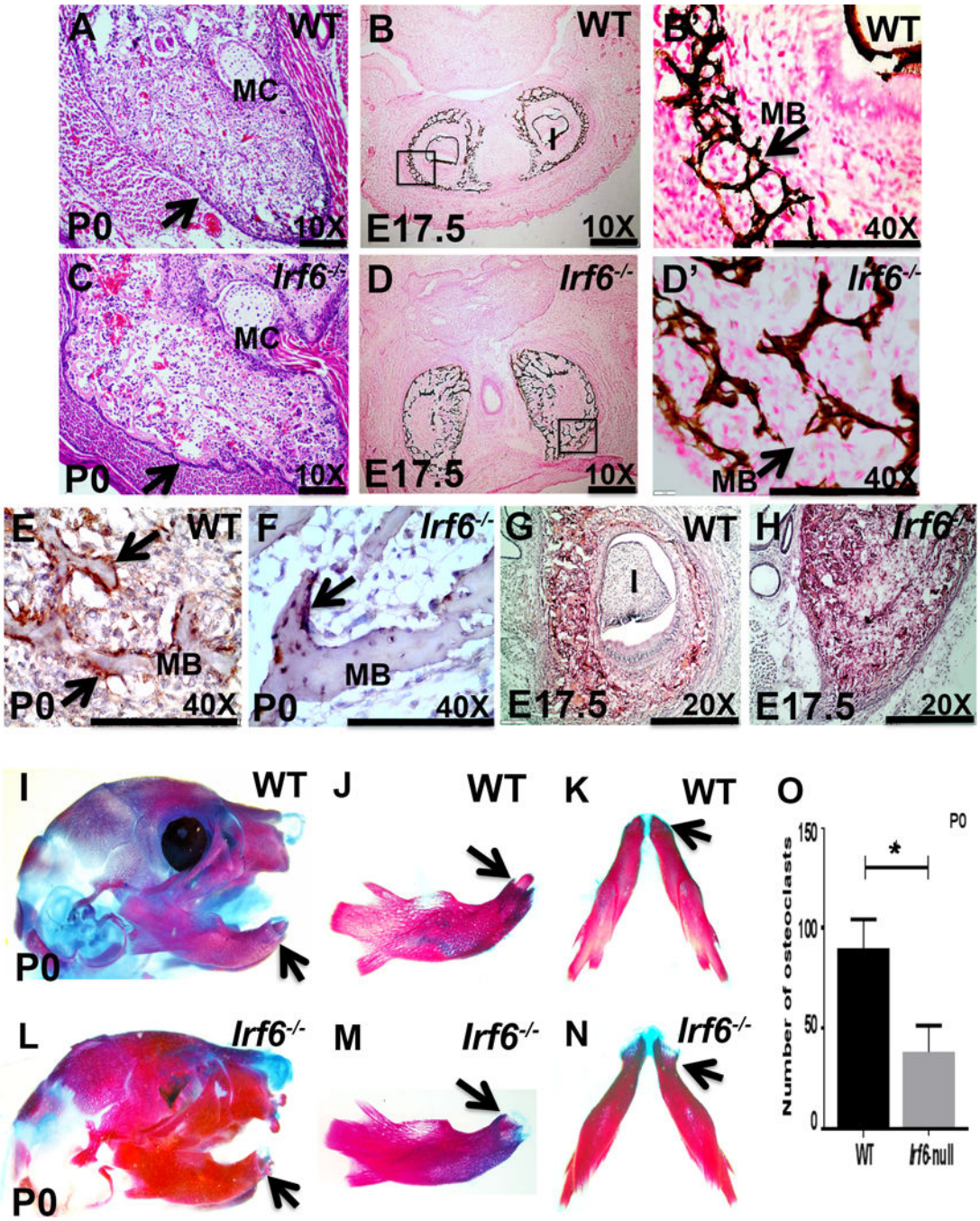

Fig. 3.

Histological, immunostaining and skeletal preparation of wild-type and *Irf6*-null tissues. H&E staining of a coronal section of WT mandibular tissues shows the trabecular bone matrix, Meckel's cartilage and periosteum (A, black arrow). In *Irf6*-null pups, the periosteum is morphologically irregular with a lobulated outer layer (C, black arrow), and the trabecular bone is disorganized with large void areas (C). The von Kossa staining of WT mandibular section shows organized matrices of calcified bone around the incisors (B, B'), while irregular and disconnected calcified bone matrices are detected in *Irf6*-null (D, D'). To

determine the osteoclastic activity, TRAP immunostaining was conducted on WT tissues and shows enrichment along the newly formed bone matrix (E), while the number of stained osteoclasts is reduced in *Irf6*-null mandibular bone (F). Alkaline phosphatase assay shows no difference in the level of staining intensity of the trabecular bone of mandible in both WT (G) and *Irf6*-null (H). Skeletal staining of newly born WT mouse appears normal (I), while *Irf6*-null mouse shows mandibular hypoplasia and fusion of skull bones (J). The isolated WT mandible shows normal structure (J, K), while *Irf6*-null mandible lacks incisors (M) and the shape is abnormal specially at the distal part and the symphysis (N). Boxes outline the higher-magnification regions in panels B' and D'. Number of TRAP+ osteoclasts is counted in the IHC images and the average number of TRAP+ osteoclasts is significantly reduced in *Irf6*-null compared to WT littermates (O). Wild-type: WT, *Irf6*-null: $Irf6^{-/-}$, I: incisor, MB: mandibular bone, MC: Meckel's cartilage. Scale bars = 100 μm.

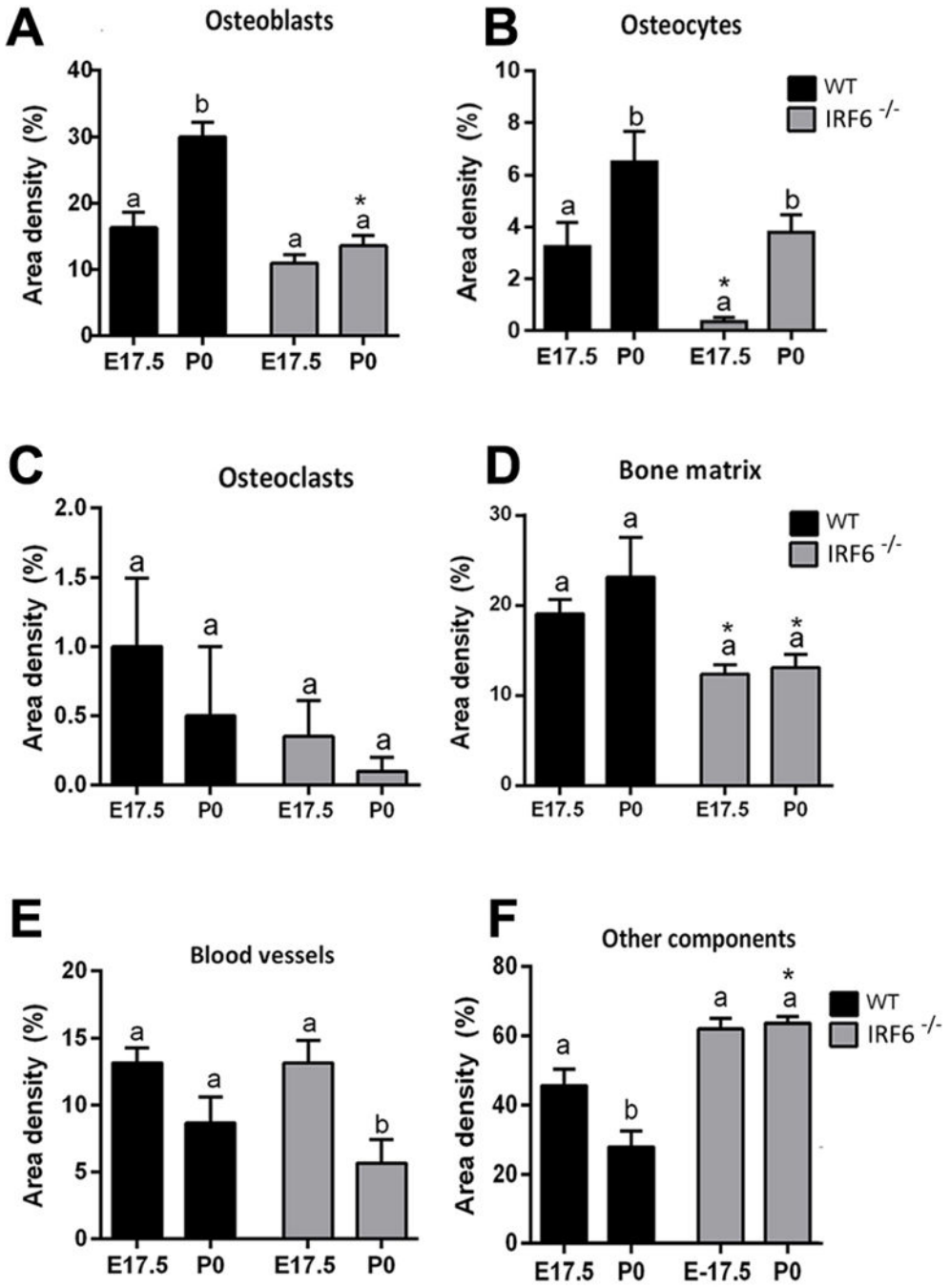

Fig. 4.

Mandibular bone components based on percentage of area density for newly born wild-type and *Irf6*-null mice. Columns in black represent data collected from counter number of WT, while columns in gray represent data collected from counter number of *Irf6*-null mandibular sections. Panel A shows the percentage of osteoblasts compared to other tissue components. Panel B measures the area density of osteocytes in the mandibular bone section by calculating the percentage of osteocytes compared to other tissue components. Panel C shows the percentage of osteoclasts in comparison to other tissue components. Panel D

shows the percentage of bone tissue components, E shows blood vessels, and F represents the other components. The results are presented as the mean area density for each evaluated cell type and structure. Different letters are used for indicating statistical differences between E17.5 and P0 time points in the same group (WT or *Irf6*-null). Symbol (*) is used for indicating statistical differences between WT and *Irf6*-null in the same time period (E17.5 or P0).

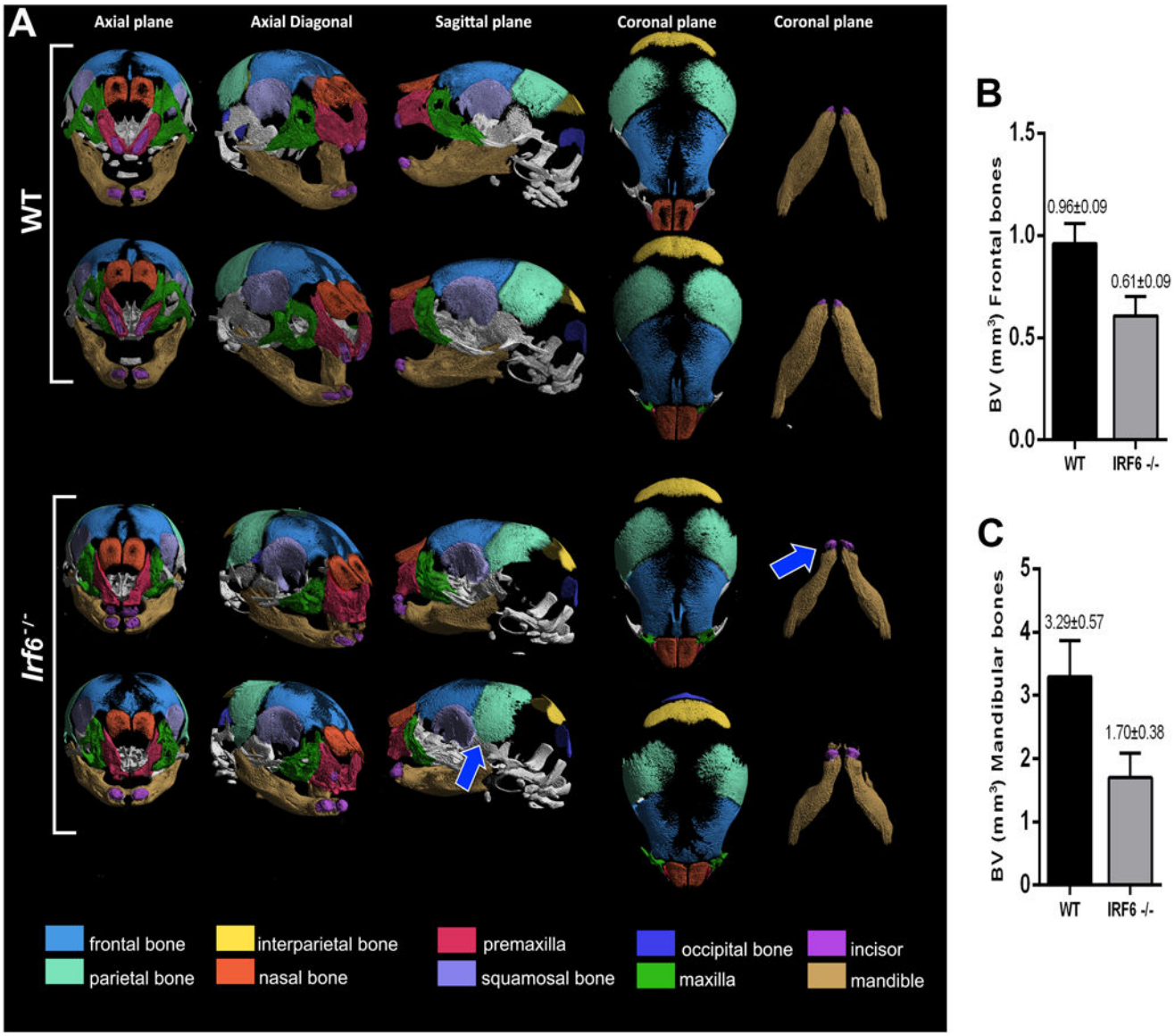

Fig. 5.

3D rendering images of micro-CT scans of wild-type and *Irf6*-null specimens. 3D micro-CT images show WT bone structure of murine postnatal heads at P0 (A, 1st and 2nd rows), and *Irf6*-null heads (A, 3rd and 4th rows) exhibit abnormal mandible and detached incisors (blue arrow). Premature closer of squamosal suture between the parietal and temporal bone is also observed in *Irf6*-null skull at P0 (blue arrow), but not in the WT skull. Total frontal (B) and mandibular bone volumes (C) are quantified and the analysis shows a reduction in the average bone volumes of *Irf6*-null mice compared to WT littermates. Wild-type: WT, *Irf6*-null: $Irf6^{-/-}$, BV: bone volume.

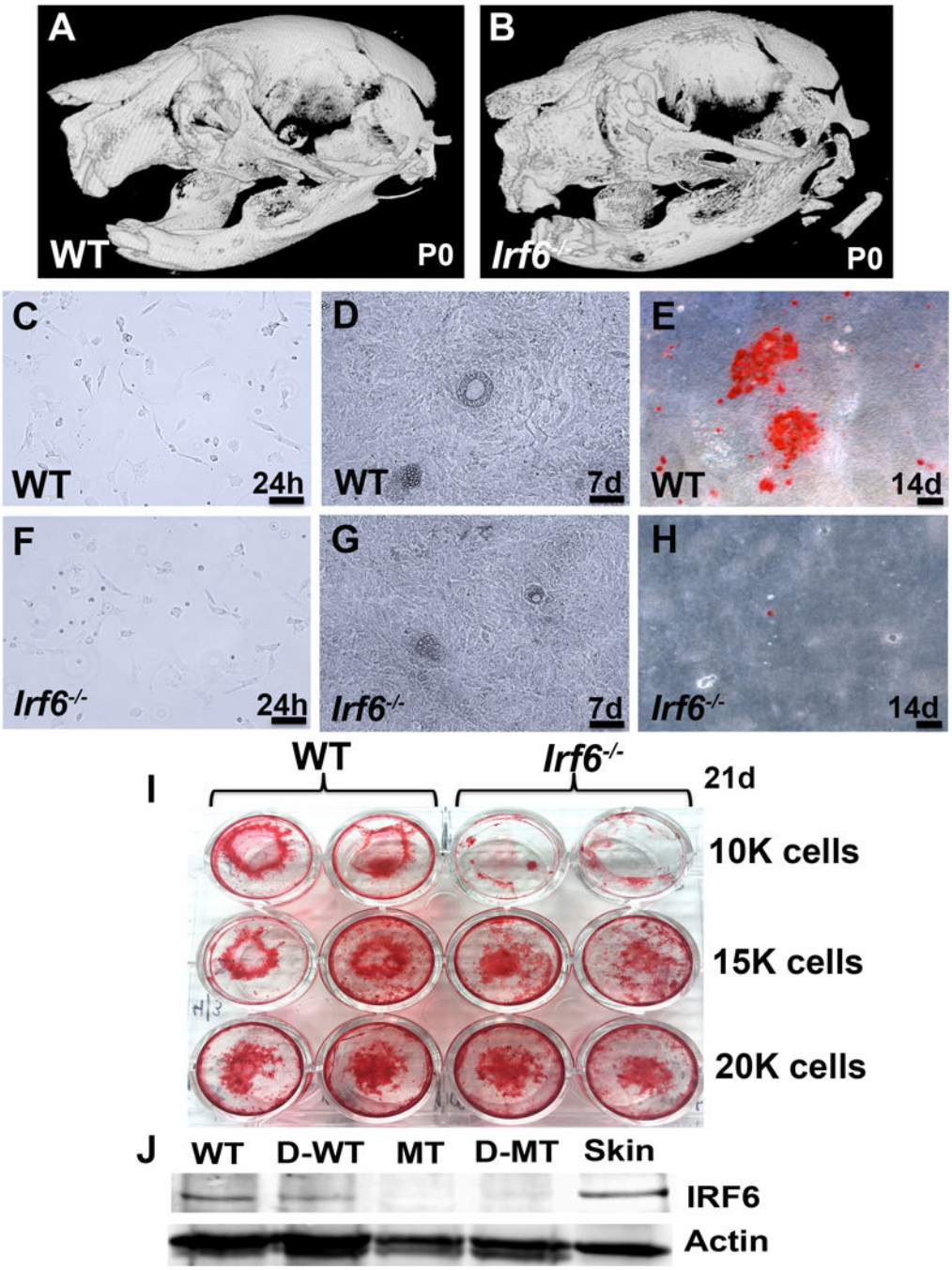

Fig. 6.

Micro-CT and isolation of calvarial primary bone cells from newborn wild-type and *Irf6*-null pups. 3D micro-CT images of wild-type and *Irf6*-null pups are taken from the same litter that was used for the isolation of calvarial primary bone cells (A, B). Fresh newborn skulls of WT (A) and *Irf6*-null (B) were used to extract osteoblast primary cells from calvarial bones and cultured in 12-well plates. A 24-hour post cultivation, the cell number is indistinguishable between WT (C) and *Irf6*-null (F). Following seven days of proliferation, confluent cells show no difference between WT (D) and *Irf6*-null (G). Alizarin red staining

for mineralized bone matrix of WT primary osteoblastic cells (E) shows a higher amount of mineralization than *Irf6*-null cells (H). After three weeks of cultivation in differentiation medium, the WT shows higher level of mineralized bone matrix compared to *Irf6*-null primary osteoblastic cells at 10K cells. However, the mineralization level is not different at higher concentrations per well (15K and 20K cells per well) (I). Western blot shows the level of IRF6 protein in bone cells cultured in normal (WT or MT cells) or differentiation media (D-WT or D-MT cells) for three weeks, and in embryonic skin at E17.5 (J). Wild-type: WT, MT: *Irf6*$^{-/-}$, d: days. Scale bars = 100 μm.

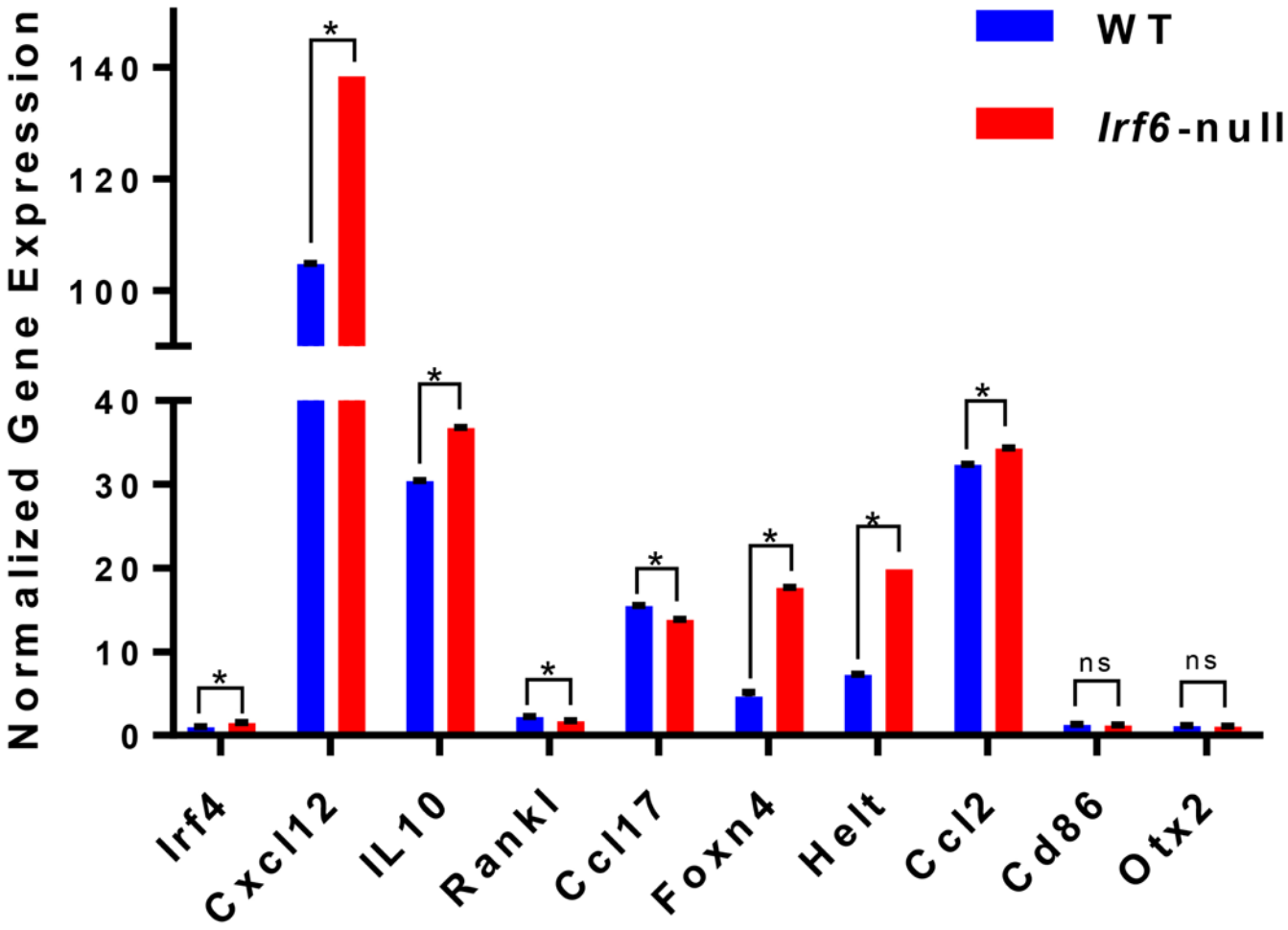

Fig. 7.

Comparative gene expression of wild-type (WT) and *Irf6*-null mouse mandibular tissue. Histogram shows the average level of mRNA expression for the 10 most differentially expressed genes out of 29 candidate genes. The results indicate that *Cxcl12*, *Il10*, *Foxn4*, *Helt*, and *Ccl2* are the most differentially altered genes in *Irf6*-null compared to WT.